THE ASTROPHYSICAL JOURNAL, 577:L63–L66, 2002 September 20

EXPERIMENTAL OBSERVATION OF ENERGETIC IONS ACCELERATED BY THREE-DIMENSIONAL MAGNETIC RECONNECTION IN A LABORATORY PLASMA

M. R. BROWN, C. D. COTHRAN, M. LANDREMAN, AND D. SCHLOSSBERG
Department of Physics and Astronomy, Swarthmore College, 500 College Avenue, Swarthmore, PA 19081
AND
W. H. MATTHAEUS
Bartol Research Institute, University of Delaware, 217 Sharp Laboratory, Newark, DE 19716
Received 2002 May 14; accepted 2002 August 12; published 2002 August 30

ABSTRACT

Magnetic reconnection is widely believed responsible for heating the solar corona as well as for generating X-rays and energetic particles in solar flares. On astrophysical scales, reconnection in the intergalactic plasma is a prime candidate for a local source (<100 Mpc) of cosmic rays exceeding the Greisen-Zatsepin-Kúzmin cutoff ($\sim 10^{19}$ eV). In a laboratory astrophysics experiment, we have made the first observation of particles accelerated by magnetic reconnection events to energies significantly above both the thermal and the characteristic magnetohydrodynamic energies. These particles are correlated temporally and spatially with the formation of three-dimensional magnetic structures in the reconnection region.

Subject headings: acceleration of particles — cosmic rays — magnetic fields — methods: laboratory — MHD — plasmas

Magnetic reconnection occurs when two bodies of highly conductive plasma bearing oppositely directed embedded magnetic fields merge (Brown 1999; Priest & Forbes 2000). In the simplest, two-dimensional picture, the interface where the inflowing magnetofluid stagnates contains a current sheet to support the curl of the magnetic field and an electric field to support the consumption of magnetic flux (see Fig. 1). Within the bulk of each inflow, the motion of the field and fluid are coupled owing to the high conductivity. At the interface, this condition no longer holds, and field lines convected into this region break and reconnect across the layer, producing a global change in field topology. The reconnection outflow, coplanar and transverse to the inflow, exits the reconnection region with a speed not exceeding that of a magnetohydrodynamic (MHD) or Alfvén wave $v_A = B/(4\pi\rho)^{1/2}$ of the coupled fluid and field. In this conventional two-dimensional geometry, the inflow and outflow regions are distinguished by field lines that meet at the center of the reconnection layer where the magnetic field is identically zero. This location is known as the X-point, and the X-line is the extension of the X-point normal to the plane and in the direction of both the electric field and the current.

The electric field at the X-point (of magnitude $E = d\psi/dt|_x$) can accelerate ions along the X-line. However, since the electric field is in the $-\boldsymbol{v} \times \boldsymbol{B}$ direction, $\boldsymbol{E} \cdot \boldsymbol{B} \equiv 0$ in the two-dimensional picture. Ions that remain precisely *on* the X-line (where $\boldsymbol{B} \equiv 0$) can be accelerated appreciably. However, relatively few ions will participate in this acceleration unless some additional features such as multiple X-lines, current sheets, or turbulent bubbles (Ambrosiano et al. 1988) trap them near the region of most intense electric field.

In three dimensions, the magnetic field can have a guiding component normal to the plane. Whether it is of external origin or self-consistently generated (Cothran et al. 2002), a guide field can enhance particle acceleration by keeping ions near the intense electric fields in the reconnection region. In fact, a viable definition of three-dimensional reconnection at a point at which $\boldsymbol{B}$ does not vanish (Schindler, Hesse, & Birn 1988; Hesse & Schindler 1988) is the appearance of an electric field along the guide field. Several models of reconnection include mechanisms for generation of out of plane fields (Shay et al. 1998). Three-dimensional solar structures have been both observed (Fletcher et al. 2001) and simulated (Birn et al. 2000). Particle acceleration in reconnection geometries is a subject of intense research (Somov & Kosugi 1997; Aschwanden, Schwartz, & Dennis 1998; de Gouveia Dal Pino & Lazarian 2000).

We report a measurement of energetic ions (protons) accelerated along the X-line coincident with the formation of three-dimensional magnetic reconnection structures. Ion detectors are spatially aligned with the anticipated X-line, and detection is temporally correlated with the magnetics. We have clear evidence of a component of the magnetic field $\boldsymbol{B}$ along the X-line. We have also mapped out the energy distribution of the ions and find it to be superthermal and super-Alfvénic. Measurements are consistent with an accelerated ion distribution characterized by a drift energy of about 90 eV and thermalized to 30 eV with $E_{\max} > 200$ eV.

There have been recent reports of reconnection-driven bidirectional sub-Alfvénic outflows observed on the Sun (Innes et al. 1997) and in the magnetospheres of the Earth (Phan et al. 2000; Oieroset et al. 2001) and Jupiter (Russell et al. 1998). There has also been significant evidence of energetic particles associated with solar flares from the *Yohkoh* satellite (Masuda et al. 1994). *Yohkoh* observations show hard X-ray sources (>50 keV) located at the loop-tops and footpoints of flares, suggesting electron acceleration along and above the loops. The maximum observed energies of particles of solar origin are ≥5 GeV (Ryan, Lockwood, & Debrunner 2000).

Magnetic reconnection may play a significant role in the acceleration of charged particles on astrophysical scales. The key feature is that the reconnection electric field is of order vB, where v is a typical MHD flow velocity and B is a typical magnetic field strength. If magnetic reconnection plays a role in particle acceleration, then maximum particle energies should scale as the reconnection electromotive force (EMF) $\mathcal{E} = \int \boldsymbol{E} \cdot \boldsymbol{dl} \sim vBL$, where L is a characteristic length of the system along the electric field (Makishima 1999). Indeed, this vBL scaling is observed in many systems where both vBL can be estimated and energetic particle measurements are available. For example, in our ex-

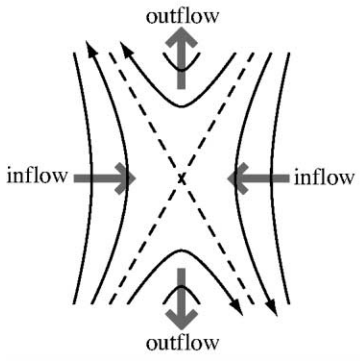

FIG. 1.—Idealized two-dimensional magnetic reconnection. Two regions contain inflowing magnetofluid with oppositely directed magnetic fields. Reconnected fields are convected away in the outflow regions. The separatrices (*dashed lines*) distinguish the four topologically distinct regions. There is a layer of current density (and Ohmic electric field) centered at the X-point.

periment $\mathcal{E} = vBL \leq (10^5\ \mathrm{m\ s^{-1}})(0.05T)(0.1\ \mathrm{m}) = 500$ V, in the solar corona $\mathcal{E} = vBL \leq (10^5\ \mathrm{m\ s^{-1}})(0.01T)(10^7\ \mathrm{m}) = 10^{10}$ V, and in exotic objects like the Crab pulsar $\mathcal{E} = v_{\mathrm{rot}}BL \leq (10^6\ \mathrm{m\ s^{-1}})(10^7 T)(10^4\ \mathrm{m}) = 10^{17}$ V.

There is clear evidence for the existence of cosmic rays with energies in excess of 10^{20} eV. Yet, energetic particles born beyond about 100 Mpc should have been slowed by the Greisen-Zatsepin-Kúzmin (GZK) energy cutoff ($\sim 5 \times 10^{19}$ eV; Cronin 1999). The GZK cutoff is due to inverse Compton scattering (photodisintegration) off the extremely blueshifted microwave background radiation at ultrarelativistic γ. The conclusion is that sources of cosmic rays with energies above the GZK cutoff must be within 100 Mpc of Earth (and there are relatively few exotic sources this close to the Local Group). Particle acceleration by three-dimensional magnetic reconnection in local, large-scale magnetic structures is a possible mechanism to exceed the GZK energy cutoff within 100 Mpc.

Several laboratory experiments have measured energetic particles in reconnection geometries, but the emphasis has been on sub-Alfvénic outflow in the two-dimensional plane (Kornack, Sollins, & Brown 1998; Gekelman, Stenzel, & Wild 1982; Ono et al. 1996). We previously observed an Alfvénic ion jet correlated with a reconnection event measured with a one-dimensional probe (Kornack et al. 1998). We also saw evidence of energetic ions with crude energy analyzers fitted with a one-parameter model (Brown 1999). Gekelman et al. (1982) directly observed outflow at up to $0.4v_{\mathrm{A}}$ in a linear slab geometry. They also observed very weak axial ion drifts ($v_i \ll 0.1v_{\mathrm{A}}$) associated with the current sheet. Gekelman & Stenzel (1985) also studied the anisotropy of the electron distribution in the reconnection layer using a novel electrostatic electron energy analyzer and found an energetic electron tail along the X-line. Ono et al. (1996) observed ion outflow up to the Alfvén speed by Doppler shifts of impurity lines in an MHD plasma. Measurements were made with a polychrometer along a chord that could be scanned radially. They found bidirectional outflow corresponding to the "slingshot" effect of newly reconnected flux. This experimental measurement corresponds directly with reconnection-driven bidirectional outflows observed on the Sun (Innes et al. 1997) and in the magnetosphere (Phan et al. 2000). Recently, Hsu et al. (2000) also measured downstream outflow in the axisymmetric device MRX ($v_i \cong 0.2v_{\mathrm{A}}$) and found plasma rotation outside the layer but low ion velocity along the X-line ($v_i \ll v_{\mathrm{th}}$).

The Swarthmore Spheromak Experiment (SSX; Brown 1999) is specifically designed to study magnetic reconnection and particle acceleration due to the controlled, partial merging of two spheromaks (see Fig. 2). We are able to generate spheromaks of either sign of magnetic helicity (right-handed or left-handed twist) on either side of the experiment. SSX is unique in that the spheromaks are generated by plasma guns away from the reconnection region (Geddes, Kornack, & Brown 1998). Neutral gas and vacuum magnetic fields are introduced at the guns, but only fully ionized plasma and embedded magnetic flux convect into the reconnection region. In addition, SSX employs a segmented copper boundary at the midplane to allow partial merging as well as allow each spheromak to relax to its own equilibrium configuration. The linear dimensions of the open chevron-shaped segments are large enough to allow significant interaction (about the spheromak minor radius $a = 0.13$ m). The segmented boundary also removes axisymmetry, making the experiment fully and inherently three-dimensional.

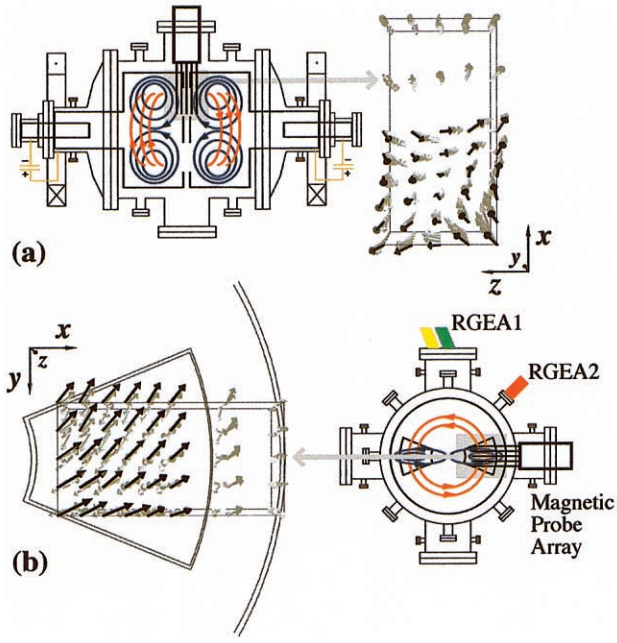

FIG. 2.—Top and end views of the SSX. Spheromaks of either helicity are formed on either side by magnetized plasma guns. The toroidal and poloidal components of each spheromak's helical field are shown in red and blue, respectively. Reconnection occurs through large slots in the back walls at the midplane. The three-dimensional magnetic probe array and retarding grid energy analyzers (*green and red*) are located at the midplane. Magnified views illustrate magnetic probe locations and data shown as arrows. The view in (*a*) is the $\hat{x}$-$\hat{z}$ plane; the view in (*b*) is the $\hat{x}$-$\hat{y}$ plane. Of the 200 $\boldsymbol{B}$ vectors, only those on facing planes are highlighted. The diameter of the chamber is about 0.6 m.

Early in the discharge, we are able to study driven reconnection as the still forming spheromaks merge at the midplane at close to the Alfvén speed (Kornack et al. 1998). Later in the discharge, the two spheromaks separately relax to nearly force-free equilibria (Geddes et al. 1998) so that we can study spontaneous reconnection along the interface between them. Typical spheromak lifetimes are 200 μs. Energetic particles and soft X-rays traverse the field-free, high vacuum gap between flux conservers to various detectors on the midplane. Special ports have been designed to view the reconnection region through a small solid angle along the X-line, so we have good spatial localization of the reconnection region. Diagnostic attention can be focused on those regions where reconnection is known to occur.

We measure electron density with a quadrature He-Ne interferometer system. Typical SSX line-averaged densities are about

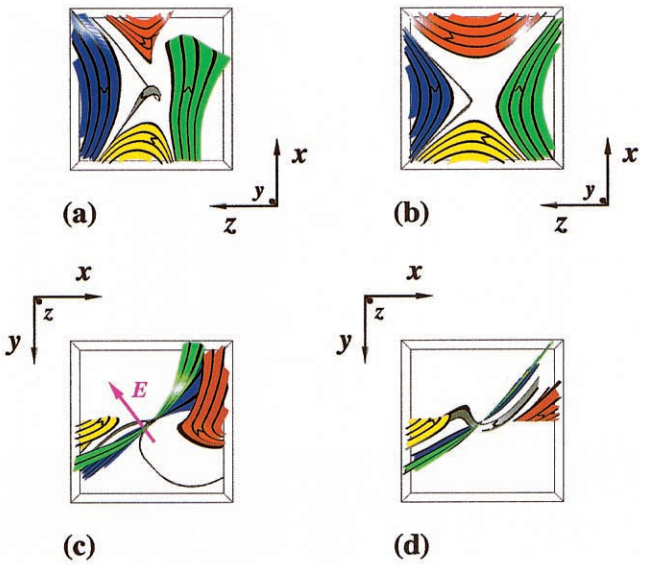

FIG. 3.—Three-dimensional reconnection. Field ribbons integrated through the three-dimensional data set from a single shot. The two views correspond to those presented in Fig. 2. The early merging phase, $t = 32$ μs, shows a flattened Y structure (*a*) that develops into a classic X structure at the later relaxation phase, $t = 64$ μs (*b*). The view in the $\hat{x}$-$\hat{y}$ plane shows a three-dimensional field line that is dynamically swept along the direction of the electric field (*c*) and develops into a swept/sheared structure (*d*). Blue and green (red and yellow) ribbons indicate magnetic field structure of inflowing (outflowing) magnetofluid. The direction of the inferred electric field is indicated. The magnetic vector data are suppressed.

$n_e = 5 \times 10^{13}$ cm^{-3}, so $c/\omega_{pi} \cong 2$–3 cm. We measure local electron density and temperature with a triple Langmuir probe ($T_e \cong 20$ eV). The ion temperature is estimated from ion energy analyzers ($T_i \cong 20$ eV). Mean magnetic fields in SSX are about $0.05T$, so $\rho_i \leq 1$ cm and $v_A = B/(4\pi\rho)^{1/2} \cong 10^5$ m s^{-1}. A proton moving at 10^5 m s^{-1} has 50 eV of energy ($E_{Alf} \cong 50$ eV). The Lundquist number is given by $S = \mu_0 \sigma v_A L \leq 1000$. The Spitzer conductivity at 20 eV is $\sigma_{Sp} = 1.7 \times 10^5 \Omega^{-1}$ m^{-1}. The electron mean free path is ≥ 0.1 m. Large-scale features of SSX plasmas are in the MHD regime ($S \gg 1$, $\rho_i/L \ll 1$, $v_A/c \ll 1$).

We measure 200 $\boldsymbol{B}$ vectors on a $5 \times 5 \times 8$ three-dimensional grid using a multiplexer technique to perform the 600 measurements at submicrosecond resolution in time and 2 cm resolution in space (Cothran et al. 2002; Landreman et al. 2002; see Fig. 2, in which we present two views of the data set). Data are obtained in a single shot. We then interpolate field lines on the three-dimensional data using fourth-order Runga-Kutta integration. Field lines are integrals of

$$\frac{dx_i}{ds} = \frac{B_i}{B},$$

where ds is an element of arc length and B is the magnitude of the field (B_i/B is the component of the unit vector along B_i). We often display a field "ribbon," consisting of a closely spaced pair of lines with the strip between colored to accentuate local twist in the field. We can also compute current density $\boldsymbol{J} = c\boldsymbol{\nabla} \times \boldsymbol{B}/4\pi$ from the magnetic data. Calibration is performed using precision Helmholtz coils and known line currents (Cothran et al. 2002).

In Figure 3, we present two views of the measured three-dimensional structure of the magnetic reconnection geometry in SSX at two times, the early merging phase, $t = 32$ μs, and the later relaxation phase, $t = 64$ μs, on a single shot. The two views correspond to those presented in Figure 2. We show field ribbons integrated through the data, which reveal a flattened Y structure (Fig. 2*a*) that develops into a classic X structure at the later relaxation phase, $t = 64$ μs (Fig. 2*b*). A field ribbon integrated near the reconnection region shows a three-dimensional field line that is dynamically swept along the direction of the electric field (Fig. 2*c*) and develops into a "swept/sheared" structure (Fig. 2*d*). This is a field line with $\boldsymbol{E} \cdot \boldsymbol{B} > 0$, where $\boldsymbol{E}$ is inferred from $-\boldsymbol{v} \times \boldsymbol{B}$ in the inflow region. The magnitude of the component of $\boldsymbol{B}$ along $\boldsymbol{E}$ is about 80 G for this shot, which is significantly greater than the systematic 20 G measurement error, and about 10% of the inflow field strength. The field line is dynamically swept into the reconnection region showing a clear signature of three-dimensional reconnection (i.e., $\boldsymbol{E} \cdot \boldsymbol{B} \neq 0$). Details of the magnetic structure are discussed elsewhere (Cothran et al. 2002; Landreman et al. 2002).

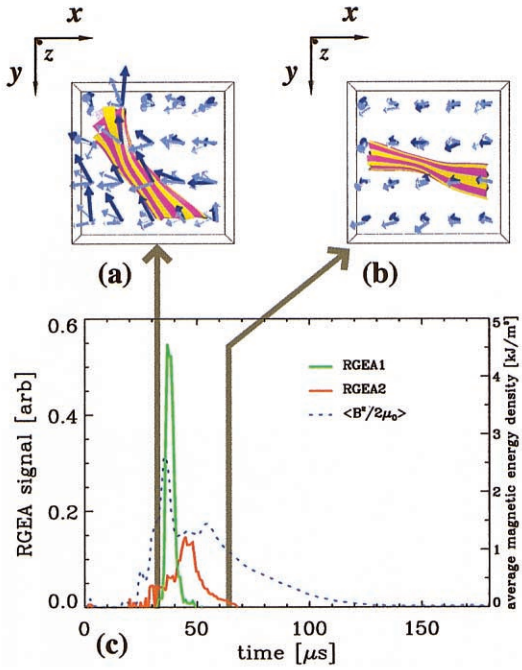

FIG. 4.—Current density and ion pulses. (*a*) Plot of the current density from Fig. 3 ($J = c\boldsymbol{\nabla} \times \boldsymbol{B}/4\pi$) during the early merging phase, $t = 32$ μs, shows an intense burst directed upward. (*b*) During the later relaxation phase, $t = 64$ μs, the current is reduced. (*c*) Ion pulses measured by our RGEAs. The early pulse (*green*) is from the RGEA aligned with the reconnection electric field. The later pulse (*red*) is from the RGEA aligned with the Alfvénic outflow. Total magnetic energy is also displayed (*dashed line*).

In Figures 4*a* and 4*b*, we present plots of the current density from the same single shot as in Figure 3 ($\boldsymbol{J} = c\boldsymbol{\nabla} \times \boldsymbol{B}/4\pi$) and at the same times. The view in Figures 4*a* and 4*b* correspond directly to Figures 3*c* and 3*d* (and Fig. 2*b*). For clarity, we show field ribbons of $\boldsymbol{J}$ (i.e., integral curves of the three-dimensional data) near the reconnection region to depict a current channel. Note that during the merging phase, the current peaks and is directed toward the top of the box (roughly the $-\hat{y}$-direction). Since locally $\boldsymbol{J} = \sigma \boldsymbol{E}$ (the inflow velocity has stagnated), this is also the direction of the local electric field as previously inferred in Figure 3*c*. Here σ is the electrical conductivity reduced from the Spitzer value by an anomaly factor. It is along this direction that we have placed one of our retarding grid energy analyzers (RGEAs). During the relaxation phase, the current drops and is no longer directed toward the energy analyzers

(roughly the $-\hat{\mathbf{x}}$-direction). The peak value of $\boldsymbol{J}$ during the merging phase is about 3.7 MA m^{-2} and is less than half that during the relaxation phase.

In Figure 4*c*, we show ion pulses measured by two of our RGEAs: the first aligned with the reconnection electric field (normal to the local reconnection layer, shown in green in Fig. 2) and the second aligned with the Alfvénic outflow (across the reconnection layer, shown in red in Fig. 2). The time history of the total magnetic energy $W_B(t) = \int B(t)^2/8\pi\, d^3x$ is also displayed. Here the integral is performed over the measured volume. The early pulse (*green*) is from the RGEA aligned with the reconnection electric field. Note that the time displayed for the intense current pulse in Figure 4*a* is just before the peak of the ion pulse of this detector, demonstrating temporal correlation between the peak of the reconnection electric field and the peak of the pulse of ions flowing in that direction (there is a few microseconds time of flight). This event is also correlated with the drop in magnetic energy W_B. The later pulse (*red*) is from the RGEA aligned with the slower sub-Alfvénic outflow. The short duration of the pulses reflect the short duration of the driven reconnection phase of the experiment. The ion flux is an order of magnitude lower during the steady reconnection phase. We want to reiterate the different physics processes associated with the two pulses: the early (*green*) pulse is due to ions accelerated by the reconnection electric field ($E \sim vB \cong 5000$ V m^{-1}) and the later (*red*) pulse is due to the slower sub-Alfvénic outflow. The directions of the two pulses are approximately 90° apart.

We are able to scan the gate voltage of the RGEAs from shot to shot. In Figure 5, we present the measured ion flux (i.e., the integrated ion distribution) as a function of gate voltage from the RGEA aligned with the reconnection electric field. Each data point is a measurement of the flux of all ions with energy exceeding the gate voltage. We show the mean and standard deviation σ for 10 shots at each voltage and fit the data with a three-parameter model (amplitude, ion temperature, and ion drift energy). To obtain this large data set (over 200 shots), the three-dimensional magnetic array was removed. The best fit (*solid curve*) is characterized by an ion distribution with drift energy of 86 $\pm$ 20 eV and thermalized to 33 $\pm$ 11 eV. The dashed lines show $\pm\sigma$ from the best fit. A sketch of the best-fit ion velocity distribution function $f(v)$ is also displayed (*upper right inset*). Note that the distribution is clearly superthermal ($E_{\rm drift} \gg E_{\rm thermal} \cong 20$ eV) and super-Alfvénic ($E_{\rm drift} > E_{\rm Alf} \cong 50$ eV) with $E_{\rm max} > 200$ eV, in contrast to earlier work (Gekelman et al. 1982; Hsu et al. 2000). Recall that the peak reconnection EMF is roughly $\mathcal{E} \cong vBL \cong 500$ V for us, consistent with this result.

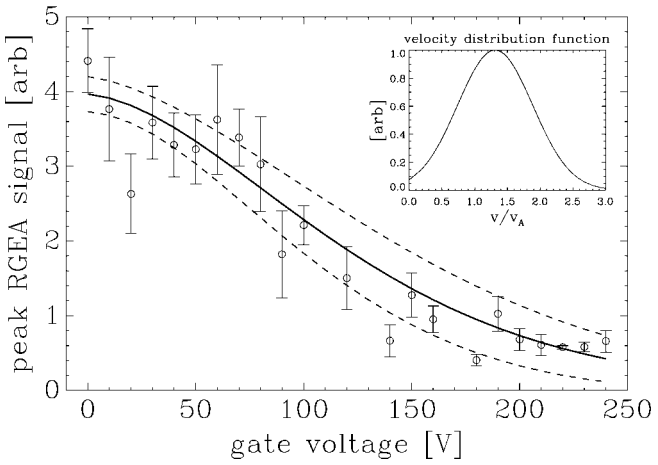

FIG. 5.—Integrated energy distribution. These measurements agree with an accelerated ion distribution characterized by a superthermal, super-Alfvénic drift energy of about 90 eV and thermalized to 30 eV. The best-fit ion velocity distribution function $f(v)$ is also displayed (*inset*).

To summarize, we have reported a measurement of ions accelerated along the X-line coincident with the formation of three-dimensional magnetic reconnection structures. RGEAs specially designed to align with the three-dimensional structures show ion pulses temporally correlated with the magnetics. We have clear evidence of a component of the magnetic field $\boldsymbol{B}$ swept and sheared along the X-line demonstrating the full three-dimensional aspect of reconnection. The energy distribution of the ions accelerated by these magnetic structures is both superthermal and super-Alfvénic. Measurements agree with an accelerated ion distribution characterized by a drift energy of about 90 eV and thermalized to 30 eV with $E_{\rm max} >$ 200 eV. This is consistent with the maximum expected energy due to the reconnection EMF ($\mathcal{E} \cong vBL \sim 500$ V).

This work was performed under Department of Energy grants DE-FG02-00ER54604 and ER54490.

REFERENCES

Ambrosiano, J., Matthaeus, W. H., Goldstein, M. L., & Plante, D. 1988, J. Geophys. Res., 93, 14383
Aschwanden, M. J., Schwartz, R. A., & Dennis, B. R. 1998, ApJ, 502, 468
Birn, J., Gosling, J. T., Hesse, M., Forbes, T. G., & Priest, E. R. 2000, ApJ, 541, 1078
Brown, M. R. 1999, Phys. Plasmas, 6, 1717
Cothran, C. D., Landreman, M., Matthaeus, W. H., & Brown, M. R. 2002, Phys. Rev. Lett., submitted
Cronin, J. W. 1999, Rev. Mod. Phys., 71, S165
de Gouveia Dal Pino, E. M., & Lazarian, A. 2000, ApJ, 536, L31
Fletcher, L., Metcalf, T. R., Alexander, D., Brown, D. S., & Ryder, L. A. 2001, ApJ, 554, 451
Geddes, C. G. R., Kornack, T. W., & Brown, M. R. 1998, Phys. Plasmas, 5, 1027
Gekelman, W., & Stenzel, R. L. 1985, Phys. Rev. Lett., 54, 2414
Gekelman, W., Stenzel, R. L., & Wild, N. 1982, J. Geophys. Res., 87, 101
Hesse, M., & Schindler, K. 1988, J. Geophys. Res., 93, 5559
Hsu, S. C., Fiksel, G., Carter, T. A., Ji, H., Kulsrud, R. M., & Yamada, M. 2000, Phys. Rev. Lett., 84, 3859
Innes, D. E., Inhester, B., Axford, W. I., & Wilhelm, K. 1997, Nature, 386, 811
Kornack, T. W., Sollins, P. K., & Brown, M. R. 1998, Phys. Rev. E, 58, R36
Landreman, M., Cothran, C. D., Brown, M. R., Kostora, M., & Slough, J. T. 2002, Rev. Sci. Instrum., submitted
Makishima, K. 1999, Astron. Nachr., 320, 163
Masuda, S., Kosugi, T., Hara, H., Tsuneta, S., & Ogawara, Y. 1994, Nature, 371, 495
Oieroset, M., Phan, T. D., Fujimoto, M., Lin, R. P., & Lepping, R. P. 2001, Nature, 412, 414
Ono, Y., Yamada, M., Akao, T., Tajima, T., & Matsumoto, R. 1996, Phys. Rev. Lett., 76, 3328
Phan, T. D., et al. 2000, Nature, 404, 848
Priest, E. R., & Forbes, T. G. 2000, Magnetic Reconnection (New York: Cambridge Univ. Press)
Russell, C. T., Khurana, K. K., Huddleston, D. E., & Kivelson, M. G. 1998, Science, 280, 1061
Ryan, J. M., Lockwood, J. A., & Debrunner, H. 2000, Space Sci. Rev., 93, 35
Schindler, K., Hesse, M., & Birn, J. 1988, J. Geophys. Res., 93, 5547
Shay, M. A., Drake, J. F., Denton, R. E., & Biskamp, D. 1998, J. Geophys. Res., 103, 9165
Somov, B. V., & Kosugi, T. 1997, ApJ, 485, 859